J. Fluid Mech. (1979), *vol.* 95, *part* 2, *pp.* 241–261
Printed in Great Britain

The effects of terrain shape on nonlinear hydrostatic mountain waves

By D. K. LILLY AND J. B. KLEMP
National Center for Atmospheric Research, Boulder, Colorado 80307

(Received 19 September 1977 and in revised form 3 January 1979)

Solutions to Long's equation for a stably stratified incompressible fluid traversing a mountain range are obtained for various terrain shapes and amplitudes when the horizontal scale is large compared to the vertical wavelength. Nonlinear lower and upper (radiative) boundary conditions are utilized and found to have a strong influence on the wave structure at large amplitudes. The results for symmetric and asymmetric mountain profiles reveal that the wave amplitude and wave drag are significantly enhanced for mountains with gentle windward and steep leeward slopes. These results confirm and explain those obtained by Raymond (1972) using a different solution method. Several results obtained by Smith (1977) from perturbation analysis are also confirmed and extended to large amplitudes. The methods are also applied to investigate the nonlinear nature of the singularity predicted by linear theory for flow over a step.

1. Introduction

We investigate and describe the structure of finite amplitude mountain waves under varying conditions of terrain height and shape. For this purpose we derive and demonstrate a rather simple technique for obtaining solutions for the two-dimensional flow of stratified fluid over large amplitude terrain. Although the technique is apparently restricted to idealized flow conditions, the results appear to aid in understanding the nonlinear structure of real mountain waves and downslope winds.

The work of Long (1953, 1955) has shown that the steady state nonlinear equations of motion, continuity, and thermodynamics for either a gas or liquid can be reduced to a second-order quasi-linear Helmholtz equation (Long's equation), provided that static stability is always positive. Further, the Helmholtz equation becomes completely linear for a Boussinesq fluid if the static stability and mean flow velocity are constant with height. While these are strong restrictions they do not necessarily bar useful theoretical investigations. One obstacle to wider application of Long's analysis has been the difficulty of obtaining solutions which fit the correct nonlinear lower boundary conditions. Only a few investigators, most notably Miles and Huppert (Miles & Huppert 1968, 1969; Miles 1968, 1969; Huppert & Miles 1969), have developed analytic solutions which satisfy this condition, and then only for rather restricted terrain conditions. Others, such as Raymond (1972), have numerically coupled solutions of Long's equation to the lower boundary using iterative procedures.

An alternative route, direct numerical simulation, can be very effective and is essential for coping with typically complex wind and temperature profiles and terrain

0022-1120/79/4365-7860 $02.00

shapes. It is, however, sensitive to various physical and numerical instabilities and to the numerical damping often used to control them (Klemp & Lilly 1978). In addition, analytic or simpler numerical solutions still seem to be more valuable for conceptual understanding.

The alternative to be presented here is to form a linear solution which fits the correct lower boundary condition, in effect by writing it in terms of co-ordinate surfaces parallel to the mountain contour. In general, co-ordinate transformations either do not preserve the linearity of the Helmholtz equation or leave it linear but with continuously variable coefficients, so that solutions must still be obtained numerically. In this case no such problems arise in the differential equations as long as interest is confined to hydrostatic flow. This restriction is appropriate if the horizontal terrain scales are large compared to the vertical wavelength, which is typically of order 10–20 km in the earth's atmosphere.

For the upper boundary a radiation condition is specified which permits only the upward propagation of wave energy. This condition is applied to nonlinear waves with some uncertainty since partial reflexions may occur through the interaction and breakdown of upward propagating modes. Nevertheless, a radiative upper boundary condition appears to provide the best available representation of hydrostatic mountain waves unless one is prepared to consider the complex processes of wave dissipation. We have implemented the radiation condition using a generalization of the technique proposed for linear waves by Drazin & Su (1975). For the nonlinear case it requires the numerical solution of a one-dimensional integral equation. For practical purposes this method may be considered as an alternative to those developed by Huppert & Miles (1969) for generalized topography and by Raymond. Although we suspect that it may be more efficient than either of those in converging to a numerical result, it is only applicable to hydrostatic flow. It may also have some advantages of conceptual simplicity, notably in the evaluation of the momentum flux integral.

Recently Smith (1977) has treated some aspects of the same problem considered here, with emphasis on the steepening of streamlines by linear and nonlinear processes. Smith obtained nonlinear solutions through a series expansion technique, with many of his results based on first-order nonlinear correction terms. There are several interesting points of comparison with the present results, though our principal emphasis will be on the effects of variable mountain shapes.

The most controversial aspect of the use of Long's equation is the question of whether its solutions are correct steady-state limits of relevant initial value problems. McIntyre (1972) has found that upstream influence, defined as a change in the mean flow profile extending indefinitely far upstream of the mountain, will occur for all topographic forcing conditions under an upper lid. From results of numerical simulation studies (Klemp & Lilly 1978), we have found that blocking, a form of upstream influence, typically occurs after the flow conditions have been adjusted to remove shearing instability, and also at levels below mountain top where the Froude number is small. None of these conditions occur in the solutions to be shown, except that at sufficiently large wave amplitudes convective instability may be present. A feature similar to upstream influence does occur over periodic mountains, however. McIntyre also noted that resonant interaction instability should occur in horizontally periodic waves, which we have also observed in numerical simulations. Thus except for the

periodic mountain case we believe, and will show evidence to document, that our solutions are generally the correct steady-state limits to relevant initial value problems.

2. Equations and method of solution

The two dimensional (x, z) inviscid Boussinesq equation of horizontal motion, the hydrostatic approximation, the incompressible continuity equation, and the equation for conservation of mass may be written conventionally as:

$$\partial u/\partial t + u\,\partial u/\partial x + w\,\partial u/\partial z + \rho_0^{-1}\,\partial p/\partial x = 0, \tag{1}$$

$$\partial p/\partial z + g\rho = 0, \tag{2}$$

$$\partial u/\partial x + \partial w/\partial z = 0, \tag{3}$$

$$\partial \rho/\partial t + u\,\partial \rho/\partial x + w\,\partial \rho/\partial z = 0, \tag{4}$$

where u and w are horizontal and vertical velocity components, p is pressure and ρ is density, with ρ_0 a reference mean density, assumed for convenience to be that of the surface streamline. Long (1953) showed that under conditions of constant mean wind velocity and static stability, solutions of the following linear differential equation are also steady-state solutions of (1)–(4):

$$(\partial^2/\partial z^2 + N^2/U^2)\,\delta = 0, \tag{5}$$

where U is the mean wind velocity and $N^2 = -g\rho_0^{-1}\,d\rho/d\bar{z}$, the Brunt–Väisälä frequency, both measured in the undisturbed (presumably far upstream) flow. The dependent variable, $\delta(x, z)$, is the vertical displacement of an air parcel from its undisturbed equilibrium height, $\bar{z}$, i.e. $\delta = z - \bar{z}$. The density and velocity fields are related to δ by

$$\rho = \rho_0(1 - N^2\bar{z}/g), \quad u = U(1 - \partial\delta/\partial z), \quad w = U\partial\delta/\partial x, \tag{6}$$

so that the streamlines are lines of constant $\bar{z}$, along which density is also constant.

The correct lower boundary condition is that

$$\delta(x, h) = h(x), \tag{7}$$

where h is the terrain height. Solutions of (5) which also satisfy (7) may be written in the real and complex forms

$$\delta(x, z) = h\cos[N(z-h)/U] + f\sin[N(z-h)/U] = \mathrm{Re}\,[H\exp(-iN(z-h)/U)], \tag{8}$$

where $H = h + if$. The real function $f(x)$ must be determined from an upper boundary condition.

The radiation condition is usually and appropriately applied in linear theory as the upper boundary condition for hydrostatic waves. It leads to solutions for which each horizontal wavenumber component has an upward group velocity, which is the apparent velocity of a 'wave packet' or beat pattern produced by several components of nearly identical wavenumber. In addition it is equivalent to the viscous solution which diminishes exponentially with height in the limit of vanishing viscosity and also to the steady-state limit of the evolving time-dependent solution which starts from rest. The radiation condition can be applied to solutions of Long's equation, because of its linear form and because horizontally propagating solutions of (1)–(4) can be obtained as solutions of (5) with U replaced by $U - \omega/k$, where ω is a temporal

frequency. For each horizontal wavenumber k and vertical wavenumber l, the wave dispersion equation may be written as

$$(\omega - Uk)^2 = k^2N^2/l^2. \tag{9}$$

The vertical group velocity, c_{gz}, is then obtained by differentiation with respect to l, i.e.

$$c_{gz} = \partial\omega/\partial l = (kU - \omega)/l, \tag{10}$$

where

$$l = \pm N/(U - \omega/k).$$

Thus for the solution with $\omega = 0$ the group velocity is upward if k and l have the same sign.

The application of this condition to a solution fitting nonlinear lower boundary conditions is now derived, essentially following and extending the treatment of the linear problem by Drazin & Su (1975); see also Miles & Huppert (1969, §5). The solution from equation (8), evaluated at the level $z = 0$ (or $z = 2n\pi U/N$, with n an integer) is

$$\delta(x, 0) = h\cos(Nh/U) - f\sin(Nh/U) = \int_{-\infty}^{\infty} \hat{\delta}(k, 0)\exp(ikx)\,dk, \tag{11}$$

where $\hat{\delta}(k, z)$ is the Fourier integral transform of the displacement height, i.e.

$$\hat{\delta}(k, z) = \frac{1}{2\pi}\int_{-\infty}^{\infty} Re[H\exp(-iN(z-h)/U)]\exp(-ikx)\,dx. \tag{12}$$

The radiation condition applied to any level requires that k/l be positive. Thus from (8) evaluated at $z = 0$ the term $\frac{1}{2}H\exp(iNh/U)$ must be the result of the Fourier integral of $\hat{\delta}(k, 0)$ over only positive k, i.e.

$$\left.\begin{aligned} H\exp(iNh/U) &= 2\int_{-\infty}^{0} \hat{\delta}(k, 0)\exp(ikx)\,dk; \\ H^*\exp(-iNh/U) &= 2\int_{0}^{\infty} \hat{\delta}(k, 0)\exp(ikx)\,dk. \end{aligned}\right\} \tag{13}$$

Drazin & Su showed that for hydrostatic flow the Fourier integrations in (13) can be carried out without evaluation of $\hat{\delta}(k, 0)$. Upon substituting (12) into (13) and reversing the order of integration, the key problem becomes the evaluation of

$$\int_{-\infty}^{0} \exp[ik(x - x')]\,dk.$$

But this is given by

$$\int_{-\infty}^{0} \exp[ik(x - x')]\,dk = \pi\Delta(x - x') + i/(x' - x), \tag{14}$$

where Δ is the Dirac delta function. This leads to the result

$$f(x)\cos[Nh(x)/U] + h(x)\sin[Nh(x)/U] = \frac{1}{\pi}\int_{-\infty}^{\infty} \frac{h(x')\cos[Nh(x')/U] - f(x')\sin[Nh(x')/U]}{x' - x}\,dx'.$$

If h and f are analytic functions of a complex argument along its real axis, then the

properties of Hilbert transforms are such that we may also write an inverse expression of the form

$$h(x)\cos[Nh(x)/U]-f(x)\sin[Nh(x)/U] = -\frac{1}{\pi}\int_{-\infty}^{\infty}\frac{f(x')\cos[Nh(x')/U]+h(x')\sin[Nh(x')/U]}{x'-x}\,dx'.$$

By algebraic manipulation, expressions for $h(x)$ and $f(x)$ are obtained in the following forms, where we now for convenience redefine l as the Scorer parameter N/U, i.e. the positive root of (10) for $\omega = 0$.

$$\left.\begin{aligned} h(x) &= -\frac{1}{\pi}\int_{-\infty}^{\infty}\frac{h(x')\sin\{l[h(x')-h(x)]\}+f(x')\cos\{l[h(x')-h(x)]\}}{x'-x}\,dx', \\ f(x) &= \frac{1}{\pi}\int_{-\infty}^{\infty}\frac{h(x')\cos\{l[h(x')-h(x)]\}-f(x')\sin\{l[h(x')-h(x)]\}}{x'-x}\,dx', \end{aligned}\right\} \tag{15}$$

or, in more compact notation,

$$H(x)\exp[ilh(x)] = \frac{i}{\pi}\int_{-\infty}^{\infty}\frac{H(x')\exp[ilh(x')]}{x'-x}\,dx'. \tag{16}$$

For each of the above integrals having integrands singular at the point $x' = x$, the Cauchy principal value is used. The linear forms derived by Drazin & Su are recovered by assuming that the Froude number, lh, is everywhere negligibly small, so that in (15) h and f are essentially Hilbert transforms of each other with alternating signs. If the group velocity were assumed to be downward instead of upward, the signs of the right-hand sides of (15) and (16) would be reversed.

The above expressions are obviously more cumbersome, both to write and solve, than those for the linear boundary condition, since the unknown function f appears inside the integral. We therefore solve the second of (15) by a numerical iterative procedure. Recognizing the singularity in the first term of the integrand, we rewrite that term as

$$f_L(x)-\frac{1}{\pi}\int_{-\infty}^{\infty}\frac{h(x')\{1-\cos l[h(x')-h(x)]\}}{x'-x}\,dx',$$

where f_L is identical to the linearized f, the Hilbert transform of h, and is typically evaluated by analytic techniques. The remaining integral and the second part of the original integral are each now regular at $x' = x$. We evaluate them by straightforward numerical quadrature, except that for some mountain profiles x and x' are transformed into different variables so that the step length can be conveniently increased for large x. The initial guess for $f(x')$ is f_L, and integration of f proceeds until convergence occurs. The adequacy of the technique is verified by then calculating $h(x)$ from the first part of equation (15), which is required to agree with the specified h to about 0·1% in most cases.

In considering the stability of these solutions, the behaviour of the Richardson number is of some interest. Using (6) the Richardson number may be defined as

$$Ri = -\frac{g\rho_0^{-1}\partial\rho/\partial z}{(\partial u/\partial z)^2} = l^2\frac{1-\partial\delta/\partial z}{(\partial^2\delta/\partial z^2)^2}. \tag{17}$$

Application of (8) yields

$$Ri = \frac{1+l(h^2+f^2)^{\frac{1}{2}}\sin[l(z-h-\lambda)]}{l^2(h^2+f^2)\{1-\sin^2[l(z-h-\lambda)]\}}, \quad \text{where} \quad \tan l\lambda = f/h. \tag{18}$$

By differentiating (18) with respect to the argument of the sine function, the minimum value of the Richardson number is found to be $Ri_{\min} = \frac{1}{2}\{1-[1-l^2(h^2+f^2)]^{\frac{1}{2}}\}$, which is greater than or equal to $\frac{1}{2}$ for $l^2(h^2+f^2) \leqslant 1$. When $l^2(h^2+f^2) > 1$, however, overturning occurs and the Richardson number takes all positive and negative values for the argument of the sine function in (18) ranging between $\pm\frac{1}{2}\pi$. Since $Ri = \frac{1}{4}$ is the upper limit for shearing instability, it is evident that shearing and buoyant instability develop simultaneously for this simple kind of mountain wave flow. This pecularity has been noted before in linear theory (Hodges 1967), for which the only difference from the above analysis is that the argument of the sine function in (18) is $l(z-\lambda)$. It does not hold, however, in the case of waves propagating in an atmosphere with vertical structure in the wind and stability fields, as for example in the multiple-layered solutions considered by Klemp & Lilly (1975). When partial reflexion occurs due to a rapid change in N or U, the combined incident and reflected modes may decrease the local static stability but increase the local shear, so that unstable Richardson numbers may occur before the overturning point.

3. Results for various mountain shapes

We now show the solutions for three idealized but representative terrain profiles and compare them with solutions obtained from the use of the linear boundary conditions, and in one case with nonlinear numerical simulations. Evaluations of wave drag as a function of mountain height and shape will then be presented and discussed. The three terrain profiles considered in this section are sinusoidal, bell-shaped and asymmetric.

The first example chosen for illustration is the continuously sinusoidal terrain described by

$$h(x) = \tfrac{1}{2}A\cos kx \tag{19}$$

where k is a positive wavenumber, arbitrary except that $k^2 \ll l^2$ if the hydrostatic equations are to remain valid. The linear approximation to $f(x)$ is the sine function, i.e.

$$f_L(x) = -\tfrac{1}{2}A\sin kx. \tag{20}$$

The nonlinear solutions for $f(x)$ are shown for various mountain heights on figure 1, normalized by division by A, the peak-to-trough mountain amplitude, and labelled by the magnitude of lA. The curve for $lA = 0$ on figure 1 is identical to f_L. As the mountain amplitude increases, $-f/A$ (and the scaled surface wind speed) tends to increase everywhere, but most strongly on the downslope side of the sinusoidal ridges.

We note that the nonlinear solutions for $f(x)$ in figure 1 differ from the linear solutions mainly by an additive constant. This difference implies that the mean flow has a component periodically oscillating in height. This is similar to the upstream influence predicted by McIntyre (1972) to occur with waves which are made periodic by energy trapping. Initial value solutions obtained by numerical simulation compare well with the above results. After a period of time which apparently depends on the amplitude, however, a series of short propagating but unstable waves develop. Although these

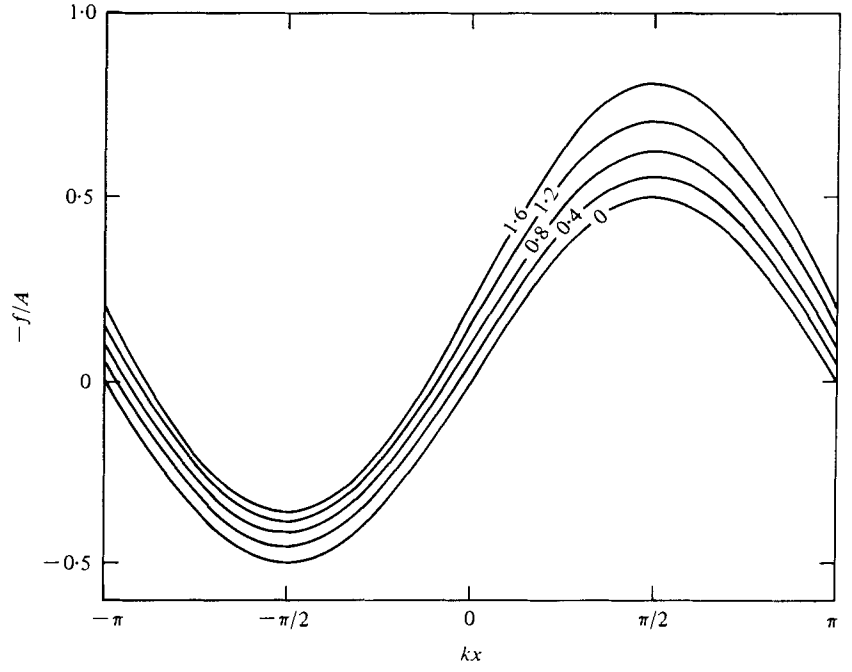

FIGURE 1. The function $f(x)/A$, as determined from equation (15), for mountain amplitudes ranging from O to $A = 1{\cdot}6\ U/N$ in steps of $0{\cdot}4\ U/N$ for the sinusoidal mountain whose profile is $h(x) = \frac{1}{2}A \cos kx$. The surface velocity perturbation equals $-Nf$.

waves ultimately destroy the solution by numerical instability, their initial development is apparently controlled by resonant interaction instability. These results are discussed in more detail by Klemp & Lilly (1978).

On figure 2 we show the streamline pattern corresponding to the values of h and f at the overturning amplitude, $lA = 1{\cdot}34$. The problem of determination of these streamlines from the displacement height solutions was discussed by Smith. The undisturbed height of a particular streamline, $\bar{z}$, can be calculated at each location and the streamlines drawn by objective analysis techniques. For greater accuracy, however, we prefer to find the displacement height as a function of x and $\bar{z}$ and then plot streamline heights as $z = \bar{z} + \delta(x, z)$. The solution is obtained iteratively by setting the function equal to zero

$$F_n = z_n - \bar{z} - \delta(x, z_n) \tag{21}$$

through repeated application of the extrapolation formula

$$z_{n+1} = z_n - (z_n - z_{n-1})\, F_n/(F_n - F_{n-1}). \tag{22}$$

The function $z_n(x, \bar{z})$ converges to z as $F_n \to 0$ and is the height of a streamline whose undisturbed height is $\bar{z}$. A slightly more elaborate procedure is required when z is multiple-valued, i.e. when the streamline amplitude has exceeded the overturning point. For all of the flow fields displayed in this section, the streamlines are plotted in the range $0 \leqslant l\bar{z} \leqslant 3\pi$.

Examination of figure 2 reveals features of nonlinear mountain waves familiar from previous research results, such as the flow over a semi-elliptical obstacle presented by

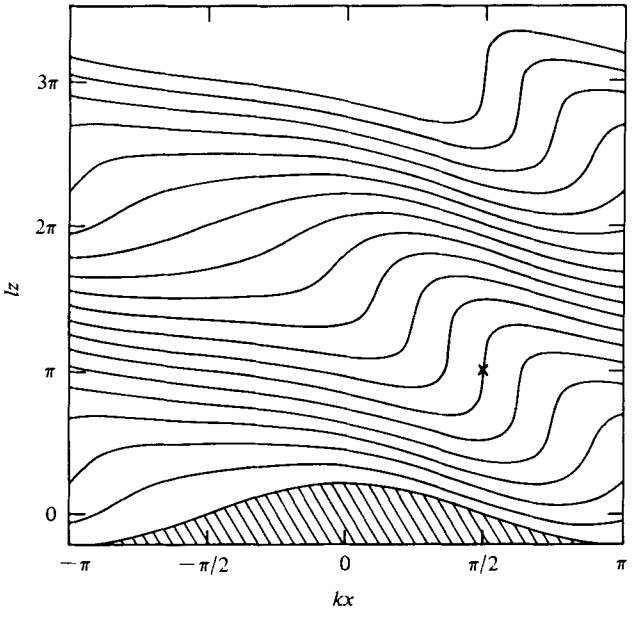

FIGURE 2. Streamlines for the nonlinear solution over a sinusoidal mountain of amplitude $A = 1{\cdot}34\ U/N$. A vertical streamline exists at the point marked ×.

Miles & Huppert (1969). The turnover point, where $u = 0 = \partial\rho/\partial x$, first occurs at $kx = \frac{1}{2}\pi$, $lz = \pi$, and recurs periodically, thus confirming the periodic steepening effect discussed by Smith. If the solution for $f(x)$ from the second of equations (16) is expanded in a power series in lA, the result to second order may be written as

$$f = \tfrac{1}{2}A(\sin kx - \tfrac{1}{4}lA).$$

Substitution of this and (19) into equation (8) produces a displacement which is identical to Smith's result from perturbation theory. From this result Smith found that vertical streamlines first occur when $lA = 1{\cdot}47$, which compares reasonably well with the value of 1·34 from the fully nonlinear solution.

For our second example we show the solutions for an isolated symmetric bell-shaped mountain, the 'Witch of Agnesi', used in several classic mountain wave studies (see, for example, Alaka 1960), with a terrain profile given by

$$h(x) = A/[1 + (x/z)^2]. \tag{23}$$

Here A is again the mountain height and a is a characteristic length scale, the distance in which the height drops by half on either side of the peak. For this case, the linear approximation to f is readily found to be

$$f_L(x) = -A(x/a)/[1 + (x/a)^2]. \tag{24}$$

Figure 3 shows nonlinear solutions for $f(x)$, again normalized by A. As in the sinusoidal case $-f$ increases everywhere from the linear profile, corresponding to an increase in surface winds everywhere, but increases most strongly just to the lee of the mountaintop.

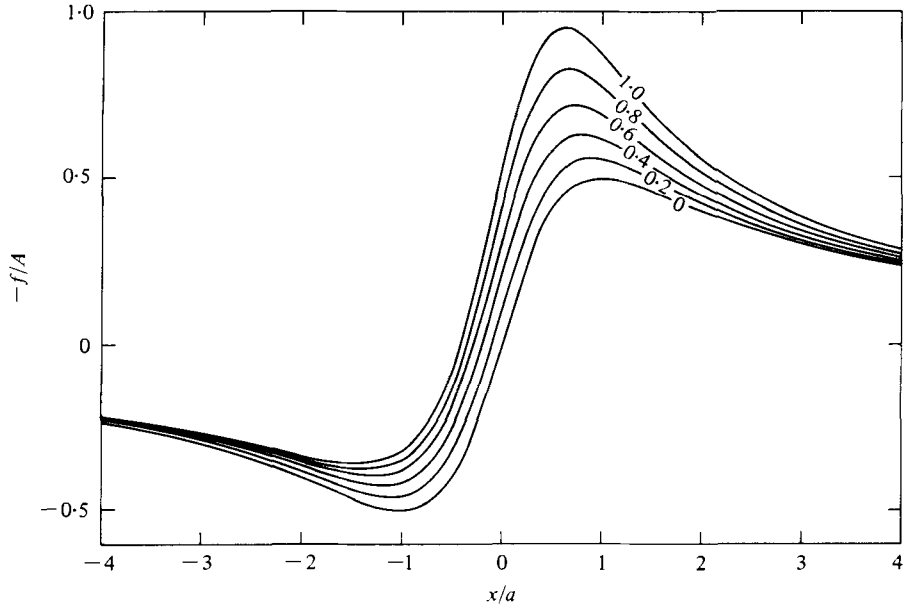

FIGURE 3. Similar to figure 1 but for the bell-shaped mountain, $h(x) = A/[1+(x/a)^2]$.

Figure 4 shows streamlines of the nonlinear solution (dashed) at a moderately large amplitude, $lA = 0{\cdot}74$, compared with those for two different linearized solutions and with the steady state result of a time-dependent numerical simulation starting from an initially unperturbed state. The first linear solution, shown by the solid streamlines in figure 4(*a*), is not the solution of Long's equation, but that of a similar equation written with $\bar{z}$ as the vertical co-ordinate. With the lower boundary conditions set (correctly) as $\delta(x, 0) = h(x)$ and the radiation condition applied in its linearized form, the solution is

$$\delta(x, \bar{z}) = h\cos l\bar{z} + f_L \sin l\bar{z}. \tag{25}$$

The streamlines depicted are those which would be produced by uniform vertical amplification of a small amplitude mountain and the streamlines over it. They correspond to probably the most common version of a linearized wave solution, but have the disadvantage that the wind speed is not proportional to the separation of streamlines. The streamlines, in fact, cross when $lA = 1$. It should be noted that Long's equation is not linear when written in x, $\bar{z}$ co-ordinates, but becomes

$$\frac{\partial^2\delta}{\partial\bar{z}^2} + \frac{N^2}{U^2}\left(1+\frac{\partial\delta}{\partial\bar{z}}\right)^3\delta = 0.$$

The solution shown by the solid streamlines on figure 4(*b*) is obtained from Long's equation with the correct nonlinear lower boundary condition but with a linearized radiation condition. The displacement height, prescribed as a function of z, is for this case

$$\delta = h\cos l(z-h) + f_L \sin l(z-h). \tag{26}$$

This solution differs from the nonlinear solution (8) only by the difference between f and f_L. By comparison to the previously depicted linear solution, the streamlines for

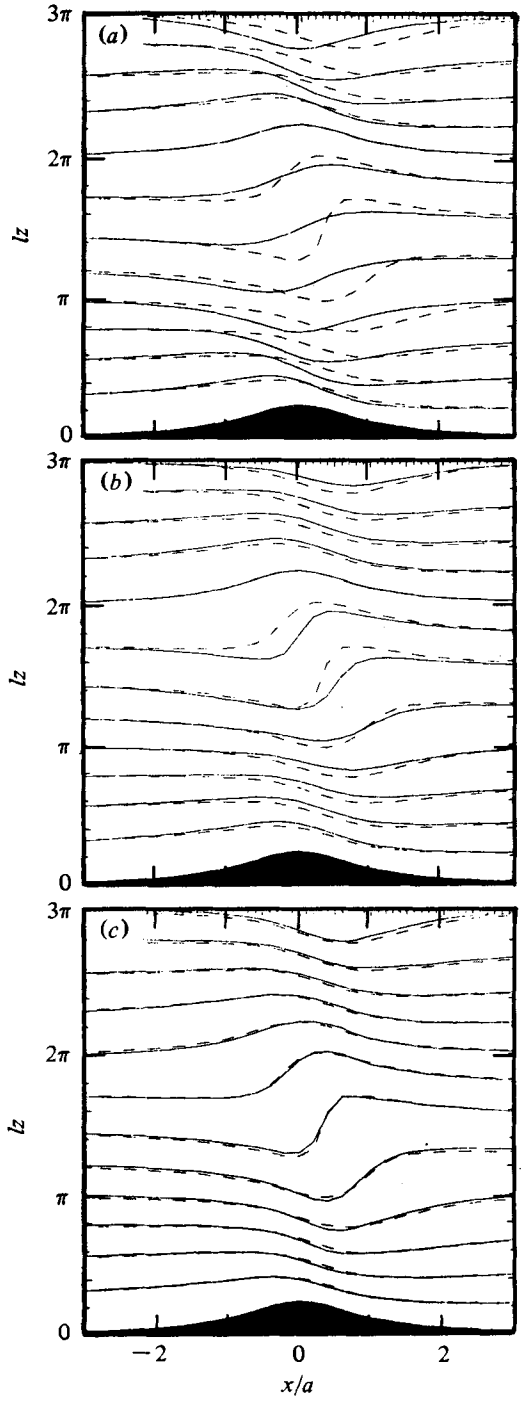

FIGURE 4. Streamlines for the nonlinear solution over a bell-shaped mountain of amplitude $A = 0{\cdot}74$ (dashed), compared with (solid) streamlines for: (*a*) a small amplitude linear solution amplified to match the above mountain height; (*b*) a solution of Long's equation with a linearized radiation condition; (*c*) the steady state result of a nonlinear time-dependent simulation.

this case are qualitatively more similar to those of the fully nonlinear flow, showing strong steepening at the right places. Also they never cross each other and the velocity is always inversely proportional to their spacing. The maximum perturbation amplitude of the velocity components is, however, somewhat smaller than that for the fully nonlinear case, and the turnover point occurs at $lA = 1$ instead of the correct value $lA = 0{\cdot}85$, as first deduced by Miles & Huppert (1969).

The dashed curve in figure 4(*c*) is the result of a numerical simulation we carried out to show the relationship of the Long's equation solutions to those resulting from the solutions of initial value problems. The methods used have been described in detail by Klemp & Lilly (1978, see §§2, 3). A thermodynamic variable is used as the vertical co-ordinate, one isoline of which is then required to follow the terrain. For comparison with the steady state solution an incompressible formulation is used, for which the relevant thermodynamic variable is the specific volume α. Klemp & Lilly's equations of one-dimensional horizontal motion, continuity, and hydrostatic balance (equation (43)) may then be written in α co-ordinates in the form

$$\frac{\partial u}{\partial t}+\frac{\partial}{\partial x}\left(\frac{u^2}{2}+gz-p\alpha\right)=F, \tag{27}$$

$$\frac{\partial}{\partial t}\left(\frac{\partial p}{\partial \alpha}\right)+\frac{\partial}{\partial x}\left(u\frac{\partial p}{\partial \alpha}\right)=0, \tag{28}$$

$$\alpha\frac{\partial p}{\partial \alpha}+g\frac{\partial z}{\partial \alpha}=0, \tag{29}$$

where F is a viscous drag term. The terrain height is specified at $\alpha = \alpha_0$, which allows $(\partial z/\partial \alpha)$ to be integrated upward to give $z(x, \alpha, t)$. Determination of the pressure field requires an upper boundary condition. Since we know of no numerically stable way to specify a radiation condition, we apply a rigid-lid condition at the top but also incorporate a viscous damping term in (27), i.e.

$$F = \nu\partial^2 u/\partial x^2, \tag{30}$$

where ν is specified as an increasing function of height in the upper portion of the domain. The optimal specification of this term is important to the results, as discussed in some detail by Klemp & Lilly. For the solutions presented here ν is given by

$$\nu = \nu_T \sin^2\left(\frac{\pi}{2}\frac{\alpha-\alpha_1}{\alpha_T-\alpha_1}\right),$$

where $\nu_T = 5aU$, and α_T and α_1 correspond to height of $lz = 7\pi$ and $lz = 3\pi$, respectively, in the undisturbed flow. Thus the damping layer is two vertical wavelengths deep.

Equations (27)–(29) are numerically formulated using finite intervals of x, α, and t, and applying centred second-order finite difference algorithms. The initial condition chosen is generally one of only horizontal motion, with a specified profile of $u(\alpha)$ and $z(\alpha)$. In order to avoid large transients the terrain profile is initialized with zero amplitude and required to grow at a constant rate until it attains the desired amplitude. Proper formulation of the upstream and downstream condition to avoid instabilities, reflexion, and uncontrolled drifting is important also, and is described in detail by

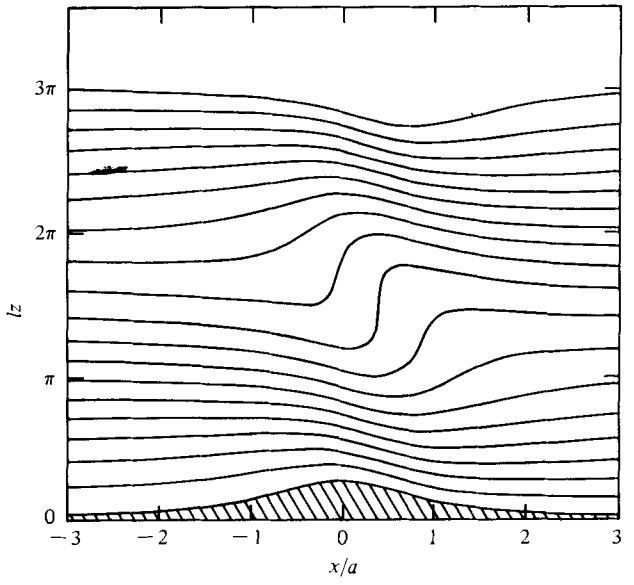

FIGURE 5. Similar to figure 2 for the bell-shaped mountain at the overturning amplitude $A = 0{\cdot}85\,U/N$.

Klemp & Lilly. For the present result we integrated over the region $|x/a| < 48$, $lz < 7\pi$, with a mesh spacing of $0{\cdot}1\,a$ in the horizontal and an α increment equivalent to $\pi/8l$ in z.

Comparison of the two sets of streamlines in figure 4(*c*) shows that they are much closer together than are either to the streamlines for the linearized equations, so that the nonlinear radiation condition leads to apparently superior results. The differences between the Long's equation and initial value solutions are not quite negligible, however. We believe them to be mainly due to inadequacies of the numerical model, especially the inability of the upper viscous layer to completely simulate a radiation condition. Klemp & Lilly show that the optimal design of that layer depends on the horizontal wavelength content of the propagating modes. As the mountain amplitude increases, the waves become relatively richer in short wavelength components, whose greater vertical group velocities allow them to pass through the viscous layer and reflect off the upper boundary with less attenuation.

Figure 5 shows streamlines for the fully nonlinear solution at overturning amplitude, $lA = 0{\cdot}85$. The first vertical streamline occurs a little downstream of the mountain top at $lz = \frac{3}{2}\pi$. Strong steepening is mostly confined to the flow over the lee side of the mountain. This feature will be compared with the flow structure over asymmetric mountains.

The third, and in some respect most interesting case to be considered is obtained by using the f_L function of equation (24) for the terrain profile, thus producing for $A > 0$ an asymmetric mountain with a sharp descent near $x = 0$ and a more gradual ascent for $|x/a| \gg 1$, with the reverse for $A < 0$. For the linear case, the solution will be identical to that of the bell-shaped mountain but displaced upward or downward by $\frac{1}{4}$ vertical wavelength. Solutions for f are shown in figure 6 and the streamline pattern at large amplitudes (in this case the value $lA = 0{\cdot}85$ at which overturning first occurs

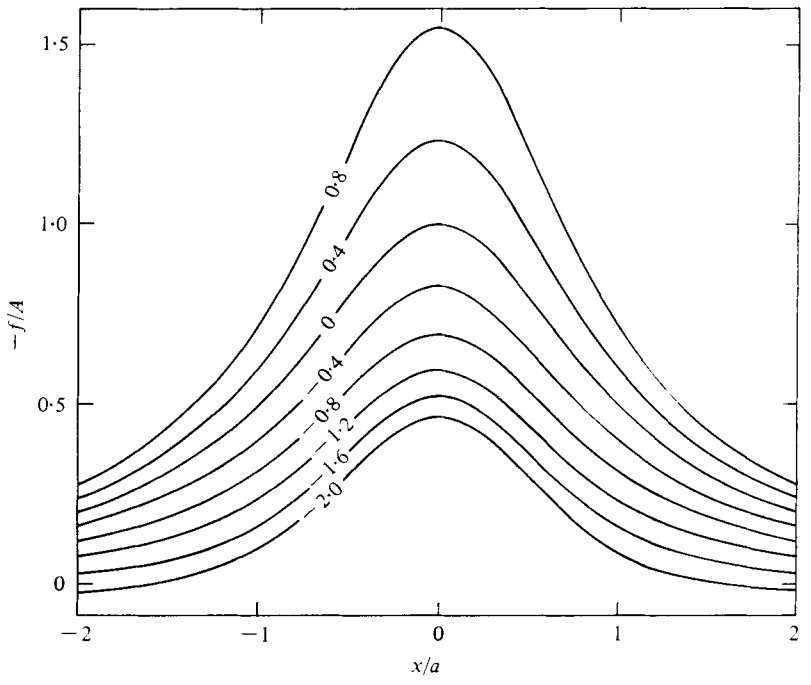

FIGURE 6. Similar to figure 1 for the asymmetric mountain, $h(x) = -A(x/a)/[1+(x/a)^2]$ Positive values of A correspond to sharp downslope and negative values to sharp upslope. Overturning occurs first at $A = 0{\cdot}68\,U/N$ and $A = -1{\cdot}97\,U/N$.

over the symmetric mountain) are shown on figures 7 and 8. The important feature is the difference between sharply rising and descending mountain slopes. For small amplitude the solutions are completely reversible with reversed mountain slope, but as the terrain amplitude grows the amplitude of f (and of the surface wind speed disturbance) grows substantially faster than linearly for a sharply descending mountain, and substantially slower for a sharp ascent. This behaviour and some of the more subtle phase changes are similar to the changes in f observed on the upstream and downstream sides of the sinusoidal and bell-shaped mountains. If the direction of the mean flow were reversed, the asymmetric mountain shapes would, of course, reverse their roles.

On figure 9 we show the streamlines for the ascending mountain at its overturning amplitude. Here the flow bears some resemblance to 'blocking', but with a limited upstream extent. For larger amplitudes it separates from the mountain.

These results confirm, extend and explain those obtained by Raymond (1972) who showed in one case that a steep lee slope produced a stronger response than a steep windward slope. Smith also showed results for asymmetric mountain shapes, with similar tendencies to those shown here. Smith interpreted his results as indicating superposition of the first-order nonlinear wave steepening on the lee side of a symmetric mountain onto the linear steepening produced by the mountain profile itself.

We offer a slightly more complete, though mainly geometric, explanation for the effects of mountain asymmetry on wave amplitude. The key is the recognition, from Smith's analysis and our figures 2 and 5, that nonlinear streamline steepening always

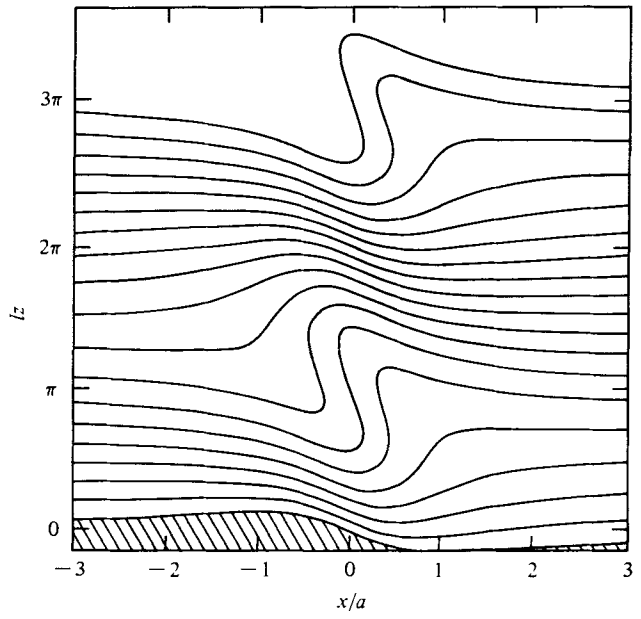

FIGURE 7. Similar to figure 2 but for the sharply descending asymmetric mountain, with $A = 0{\cdot}85\,U/N$, the overturning amplitude for the bell-shaped mountain profile.

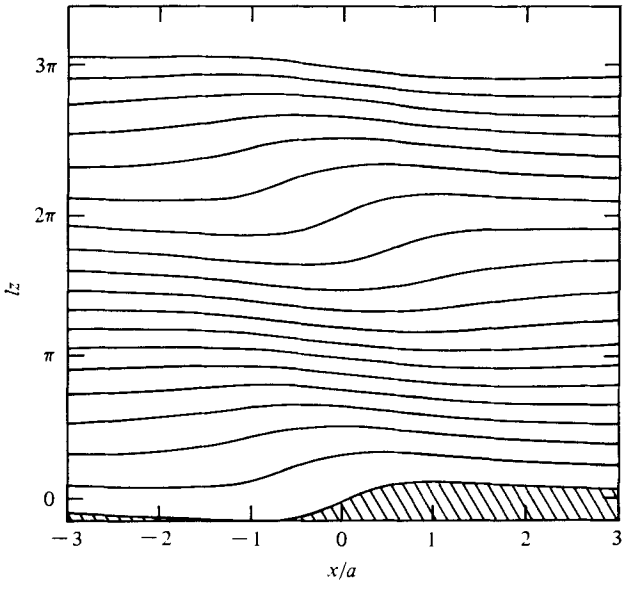

FIGURE 8. Similar to figure 7 but for the sharply ascending mountain, with $A = 0{\cdot}85\,U/N$.

occurs in a sharply upsloping flow. At the level where this is maximized (one-half vertical wavelength up for the sinusoidal mountain, three-fourths for the bell-shape) the displacements and potential energies are maximized and the horizontal velocity perturbations and kinetic energies minimized. Converse results hold one-half vertical wavelength above and below this level. For each of the solutions presented, for example

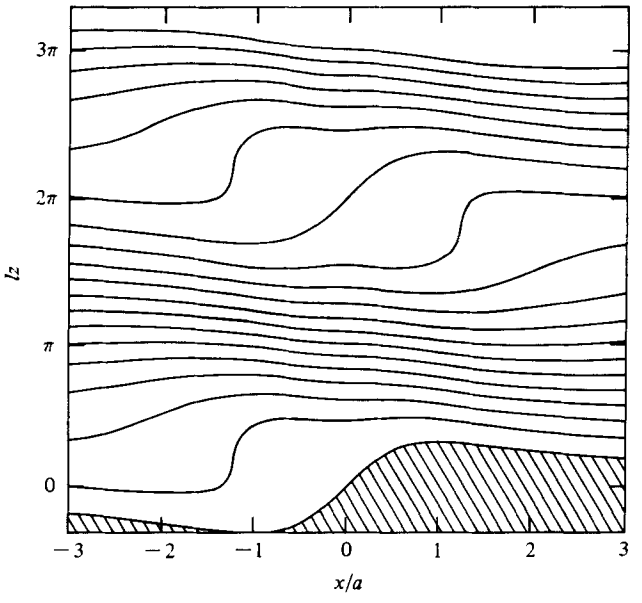

FIGURE 9. Similar to figure 8 but for the overturning amplitude $A = -1{\cdot}97\,U/N$.

figure 5, a displaced but otherwise identical flow pattern could be produced if the mountain shape were replaced by that of any streamline above it. If the streamline were the one where the displacements are minimized, then everywhere above it the flow would have a greater displacement amplitude and smaller velocity amplitude than those at the mountain surface. In effect that is what we have done by choosing the sharp downslope profile of figure 7 to be identical to the linear case streamline one-fourth wavelength above the surface of the bell-shaped mountain. On the other hand by choosing a sharp upsloping mountain profile of a given amplitude, we minimize the displacements everywhere above it, and the velocity amplitude along it, thus minimizing total energy and, as we will show, wave drag.

Our results qualitatively resemble the observed behaviour of air flow over large mountains. In the U.S. and Canada the mean wind direction at the altitudes of higher mountains is from the west. The strongest mountain wave effects, including severe downslope winds, seem most often to be observed in the lee of mountain ranges with gradual rises on their western sides and rapid descents to the east, such as the central Colorado Rockies west of Denver (Klemp & Lilly 1975), the Canadian Rockies west of Calgary (Lester 1976), and parts of the Sierra Nevada (Alaka 1960). On the other hand, the Wasatch Mountains near Salt Lake City have the opposite configuration. Here strong mountain waves and downslope winds occur only on the western slopes during the occasional periods when the mean flow is from the east (Harrison 1965). For comparison, the maximum surface wind speed for the bell-shaped mountain of figure 5 is 1·72 times the mean flow, while over the sharply descending mountain of figure 7 it is 2·36 times the mean flow. For the sharply ascending mountain of figure 8 it is everywhere less than the mean flow.

Probably the most important quantitative measure of mountain wave intensity, both for its effects on local meteorology and on larger scales of motion, is the exchange

of momentum between the atmosphere and the sloping lower boundary. The wave drag is the force which the earth exerts on the atmosphere through differential pressures on the windward and leeward slopes, and is given by the integral along the surface of ph', where $h' = dh/dx$. Large values of wave drag are associated with strong mountain wave effects, including wave-induced turbulence and downslope windstorms (Klemp & Lilly 1975). Since wave drag propagates vertically as wave momentum flux, the exchange may actually occur at some upper level where turbulent breakdown occurs, thus causing a removal of momentum from the atmospheric general circulation (Bretherton 1969; Lilly 1972).

To obtain the wave drag, we must first evaluate the surface pressure. From equation (1) in the steady state and (5)–(6) a Bernoulli equation holds, so that at $z = h$,

$$p = (-\tfrac{1}{2}\rho_0)(u^2 + N^2h^2) = -(\tfrac{1}{2}\rho_0 U^2)[(1-lf)^2 + l^2h^2]. \tag{31}$$

Thus the wave drag of the earth on the atmosphere is

$$D = -\int_{-\infty}^{\infty} p(x,h)\,h'dx = \rho_0 U^2 \int_{-\infty}^{\infty} [lf - l^2f^2/2]\,h'dx, \tag{32}$$

where we assume that the surface terrain heights far upstream and downstream of the mountain are equal. In the case of periodic terrain we will calculate the integral only over a single wave period, however. The first term of the integral is identical in form to the result obtained from the usual linear theory, except for the difference between f and f_L. This term is always positive if $U > 0$ (Drazin & Su 1975). The second is a product of the present analysis, significant only for large amplitude terrain, and may vary in sign, depending on the mountain shape.

Figure 10 shows the wave drag, plotted as the ratio of its value to that of the linear solution, for various terrain shapes and for amplitudes up to and above the overturning amplitude, shown as a $\times$ on each curve. For each of the mountain profiles the drag for the linear lower boundary condition is

$$D_L = -\rho_0 U^2 \int_{-\infty}^{\infty} lf_L\,h'dx = \tfrac{1}{4}\rho_0 \pi l A^2 U^2. \tag{33}$$

From these results we see the strong effects of mountain asymmetry in the nonlinear solutions. For the symmetric and sinusoidal terrain the wave drag is mainly proportional to the square of the mountain height, with 4th- and higher-order terms becoming significant only for amplitudes close to overturning. The drag of the asymmetric mountains has a large cubic term, which is not present in either the symmetric nonlinear or asymmetric linear solutions. On the other hand, if one averages the wave drag from the upslope and downslope asymmetric mountains, the resulting drag curve is similar to (though larger than) that for a symmetric mountain. From this viewpoint also one can interpret the flow over the asymmetric mountain with sharp downslope as qualitatively similar to that over the downslope side of a symmetric mountain, and similarly for the sharp upslope case. This is not inconsistent with Smith's interpretation of the additive effects of nonlinear wave steepening and mountain asymmetry, but it shows the importance of the tendency for most vertical motion to occur on the downslope side of the mountain in highly nonlinear flow.

We have also plotted, as dashed curves, the values obtained from use of the nonlinear lower boundary condition and the linearized radiation condition, using $f(x) = f_L$

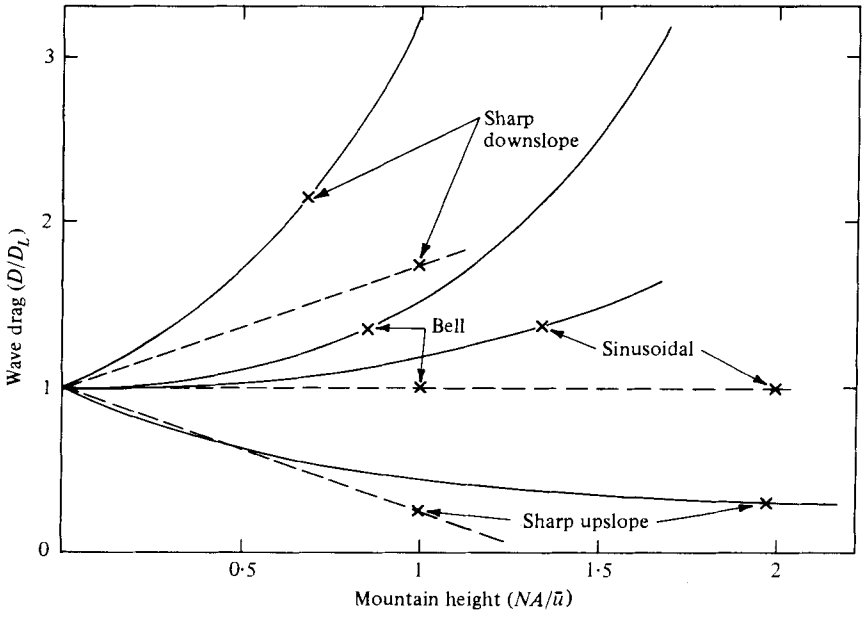

FIGURE 10. Wave drag D plotted as the ratio of its value to that of the linear solution D_L for various mountain shapes and amplitudes. The solid curves are for the complete solution while the dashed curves use the linearized radiation condition $f = f_L$. Overturning occurs at the points marked ×.

in equation (32). These results tend to be consistent with the impressions obtained from inspection of the f profile and the flow streamlines. The drag is generally less than that obtained from the correct radiation condition but the principal elements of flow asymmetry and periodic wave steepening are captured.

4. The flow over a step mountain

One of the more striking conclusions of linear mountain wave theory is the prediction for flow over a one-sided or step mountain, that is one for which the displacement never returns to zero on the lee side. As pointed out by Bretherton (1969) the steady state horizontal velocity function $f_L(x)$ is singular, i.e. infinite, for this case. The singularity is logarithmic in nature and can be removed in several ways. Let us suppose, for example, that the mountain shape is given by

$$h(x) = A[\tfrac{1}{2}\pi + \tan^{-1}(x/a)].$$

If an initial value problem is considered, with displacement starting from zero everywhere except along the surface, then the amplitude of f_L increases like $\ln(Ut/a)$, and thus remains finite for all finite time. If a vertical viscosity coefficient ν is added to the equations, then the steady state amplitude of f_L becomes proportional to $\ln(aU/\nu)$. Horizontal viscous terms do not, however, remove the singularity. If rotational effects are included the downstream velocity is bounded but the cross-stream component, and therefore the total kinetic energy, still approaches logarithmic infinity. Of course the fact that all mountains are of limited lateral extent and that the singularity only exists for line-symmetric ranges reduces the physical interest considerably. Smith

(1979) points out that a similar problem occurs in aerodynamic theory for an infinitely long and wide airfoil.

Despite the ultimately non-physical nature of the singularity we felt that it would be of some interest to explore its nonlinear aspects, by determining from the Long's equation model whether the singularity remains present for finite amplitude mountains. Given the fact that the wave energy must ultimately come from that of the mean flow, it might seem unlikely that this energy would increase indefinitely with mountain width. To investigate the question we used a two-scale mountain, developed by superimposing the left half of a wide bell-shaped mountain on the right half of a narrow one, or vice versa, i.e.

$$h(x) = \begin{cases} A/(1+x^2/a^2) & \text{for} \quad x > 0, \\ A/(1+x^2/b^2) & \text{for} \quad x < 0. \end{cases} \tag{34}$$

This mountain has a second-order discontinuity at $x = 0$. An alternative and cleaner shape could be obtained by superimposing two arctan mountains of opposite sign, separated by a variable distance to form a table mountain, but this turned out to be less convenient numerically. For the above mountain the linear f function is given by

$$f_L(x) = -\frac{A}{2}\left\{\frac{x/b}{1+x^2/b^2}+\frac{x/a}{1+x^2/a^2}-\frac{1}{\pi}\left[\frac{\ln(x^2/b^2)}{1+x^2/b^2}-\frac{\ln(x^2/a^2)}{1+x^2/a^2}\right]\right\}. \tag{35}$$

The terms in square brackets do not appear for the normal bell-shaped mountain with $a = b$. They are responsible for the ultimate singularity, since they produce the result $f_L(0) = (A/\pi)\ln(a/b)$. A similar result holds for the table mountain.

We have obtained complete nonlinear solutions, using equation (15), for b/a ranging between 10^{-4} and 10^4. In one set of computations, the mountain amplitude was fixed at a value such that f could be assumed to be in the linear range for $a = b$ but would reach nonlinear amplitude for large b/a. In a second set, we prescribed the mountain amplitude as a function of b/a such that the maximum value of f_L approaches a constant as the ratio becomes very large or very small. In order to evaluate the integral accurately we carried out a polynomial transformation of the horizontal dimension, so that adequate numerical resolution was present throughout the domain without an unacceptably large number of integration points at large distances from the origin.

Figure 11 shows the maximum values of $f(x)$ and of $f_L(x)$ for the case with small fixed mountain amplitude, $lA = 0{\cdot}1$. The abscissa is in logarithmic coordinates, so that at large values of b/a the f_L value lies along a straight line. The nonlinear solution is everywhere greater than the linear one, and reaches the turnover point for $b/a \sim 10^6$. This increase is due to the sharply descending profile downstream, similar to the results for the asymmetric case shown in § 3. For $b/a < 1$ the nonlinear solution would be everywhere smaller than the linear case.

Table 1 shows f/f_L (maximum values) and the ratio of the wave drags, D/D_L, for the second set of computations. For these the mountain amplitude was prescribed such that $lA\,[\frac{1}{4}\pi + \ln(b/a)] = \frac{1}{4}$, for which the maximum value of f_L approaches a constant for large values of $|\ln(b/a)|$. The amplitude behaviour is such that the solutions are effectively more nonlinear at $a = b$ than elsewhere, so that the tabulated ratio initially decreases in both directions. As b/a or a/b become very large the ratios obviously converge, however, being greater than unity for the sharply descending mountain and smaller for the case of sharp ascent.

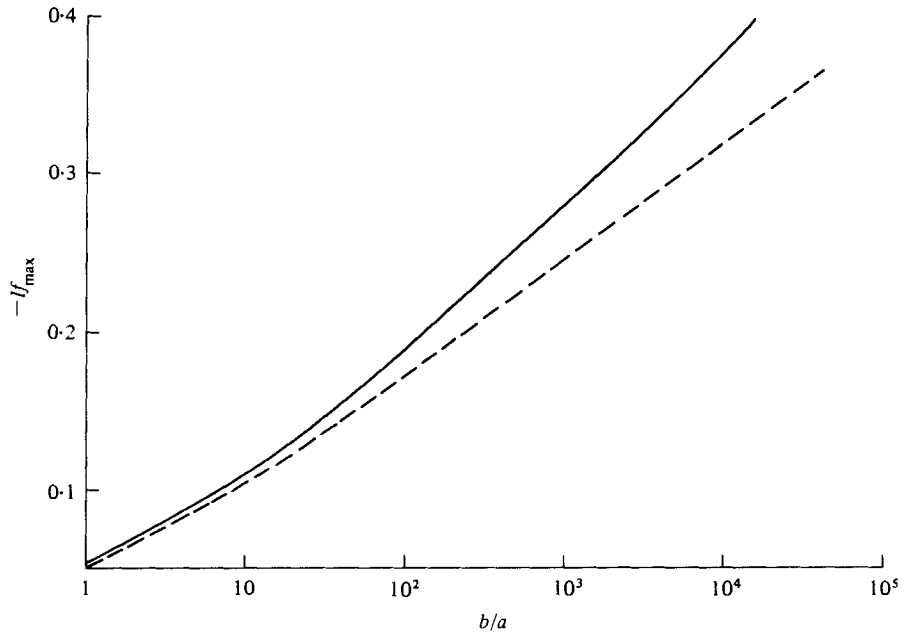

FIGURE 11. Maximum value of lf for the two-scale mountain solutions as a function of the ratio of the upstream to downstream scales. Nonlinear solutions are solid, linear dashed.

a/b	lA	lf_{Lmax}	f_{max}/f_{Lmax}	M/M_L
10^{-4}	0·079	0·250	0·883	0·899
10^{-3}	0·102	0·250	0·881	0·902
10^{-2}	0·146	0·251	0·877	0·910
10^{-1}	0·254	0·261	0·858	0·931
1	1·000	0·500	1·873	1·279
10	0·254	0·261	1·203	1·122
10^2	0·146	0·251	1·162	1·126
10^3	0·102	0·250	1·149	1·130
10^4	0·079	0·250	1·145	1·132

TABLE 1. Maximum surface wind functions and momentum fluxes for two-scale mountain solutions.

These results show that nonlinearity does not qualitatively change the nature of the singularity found for linear flow, and quantitatively changes it only in the same way as it does the solutions for bounded asymmetric mountains. Of course once overturning instability occurs a new set of physical factors enters. We expect that a realistic numerical simulation of flow over a mountain with large b/a and amplitude sufficient for overturning would develop some form of blocking after the instability occurred.

5. Conclusions

In earlier work (Klemp & Lilly 1975, 1978) we have shown how the atmospheric response to topographic forcing at hydrostatic scales is affected by the details of the atmospheric flow and thermal profiles. The above results indicate how and why that response tends to be a strong function of the shape, as well as the amplitude, of the terrain. In particular, they show that terrain with a gradual upslope and steep downslope profile is optimal for producing intense waves, strong surface winds, and large wave drag, which is explainable as a direct consequence of the geometry of nonlinear wave steepening. It is evident that the above methods can be readily applied to other mountain shapes. Extension to more general flow and stability profiles is of doubtful practicability, however, since Long's equation becomes nonlinear in most cases. It appears possible to obtain solutions for two- or three-layered atmospheres, with stability discontinuities between the layers. The interfacial boundary conditions lead to transcendental equations, however, requiring additional iterative numerical treatments.

Our method of solution allows for separate consideration of the effects of nonlinearity in both the lower and upper boundary conditions. We find that the qualitative nature of the flow, and especially its asymmetries, depends principally on satisfaction of the nonlinear lower boundary condition. Use of the linearized radiation condition permits easy determination of solutions which retain the correct qualitative properties.

We gratefully acknowledge the key contributions to this paper by George Chimonas, who pointed out the merit of using the nonlinear radiation condition, and by Philip Drazin, who encouraged formulation of a proof of its validity. The National Center for Atmospheric Research is sponsored by the National Science Foundation.

REFERENCES

ALAKA, M. A. 1960 The airflow over mountains. *Tech. Notes Wld met. Org.* no. 34.

BRETHERTON, F. P. 1969 Momentum transport by gravity waves. *Q. J. Roy. Met. Soc.* **95**, 213.

DRAZIN, P. G. & SU, C. H. 1975 A note on long-wave theory of airflow over a mountain. *J. Atmos. Sci.* **32**, 437.

HARRISON, H. T. 1965 *N.A.S.A. Contractor Rep.* NASA CR-315.

HODGES, R. R. 1967 Generation of turbulence in the upper atmosphere by internal gravity waves. *J. Geophys. Res.* **72**, 3455.

HUPPERT, H. E. & MILES, J. W. 1969 Lee waves in a stratified flow. 3. Semi-elliptical obstacle. *J. Fluid Mech.* **35**, 481.

KLEMP, J. B. & LILLY, D. K. 1975 The dynamics of wave-induced down-slope winds. *J. Atmos. Sci.* **32**, 320.

KLEMP, J. B. & LILLY, D. K. 1978 Numerical simulation of hydrostatic mountain waves. *J. Atmos. Sci.* **35**, 78.

LESTER, P. F. 1976 Evidence of long lee waves in southern Alberta. *Atmosphere* **14**, 28.

LILLY, D. K. 1972 Wave momentum flux – a GARP problem. *Bull. Amer. Meteor. Soc.* **53**, 17.

LONG, R. R. 1953 Some aspects of the flow of stratified fluids. I. A theoretical investigation. *Tellus* **5**, 42.

LONG, R. R. 1955 Some aspects of the flow of stratified fluids. III. Continuous density gradient. *Tellus* **7**, 341.

McIntyre, M. E. 1972 On Long's hypothesis of no upstream influence in uniformly stratified or rotating flow. *J. Fluid Mech.* **52**, 209.

Miles, J. W. 1968 Lee waves in a stratified flow. 1. Thin barrier. *J. Fluid Mech.* **32**, 549.

Miles, J. W. 1969 The lee-wave regime for a slender body in a rotating flow. *J. Fluid Mech.* **36**, 265.

Miles, J. W. & Huppert, H. E. 1968 Lee waves in a stratified flow. 2. Semi-circular obstacle. *J. Fluid Mech.* **33**, 804.

Miles, J. W. & Huppert, H. E. 1969 Lee waves in a stratified flow. 4. Perturbation approximations. *J. Fluid Mech.* **35**, 497.

Raymond, D. 1972 Calculations of airflow over an arbitrary ridge including diabatic heating and cooling. *J. Atmos. Sci.* **29**, 837.

Smith, R. B. 1977 The steepening of hydrostatic mountain waves. *J. Atmos. Sci.* **34**, 1634.

Smith, R. B. 1979 Some aspects of the quasi-geostrophic flow over mountains. To appear in *J. Atmos. Sci.*

Titchmarsh, E. C. 1937 *Introduction of the Theory of Fourier Integrals.* Oxford University Press.